UNeR3D: Versatile and Scalable 3D RGB Point Cloud Generation from 2D Images in Unsupervised Reconstruction

 $\label{eq:continuous} Hongbin\ Lin^{1,2,\dagger} \qquad Juangui\ Xu^{1,3,\dagger} \qquad Qingfeng\ Xu^1 \qquad Zhengyu\ Hu^2 \qquad Handing\ Xu^1$

Yunzhi Chen¹ Yongjun Hu³ Zhenguo Nie^{1*}

¹Tsinghua University ²HKUST(GZ) ³Guangzhou University

Abstract

*In the realm of 3D reconstruction from 2D images, a per*sisting challenge is to achieve high-precision reconstructions devoid of 3D Ground Truth data reliance. We present UNeR3D, a pioneering unsupervised methodology that sets a new standard for generating detailed 3D reconstructions solely from 2D views. Our model significantly cuts down the training costs tied to supervised approaches and introduces RGB coloration to 3D point clouds, enriching the visual experience. Employing an inverse distance weighting technique for color rendering, UNeR3D ensures seamless color transitions, enhancing visual fidelity. Our model's flexible architecture supports training with any number of views, and uniquely, it is not constrained by the number of views used during training when performing reconstructions. It can infer with an arbitrary count of views during inference, offering unparalleled versatility. Additionally, the model's continuous spatial input domain allows the generation of point clouds at any desired resolution, empowering the creation of high-resolution 3D RGB point clouds. We solidify the reconstruction process with a novel multiview geometric loss and color loss, demonstrating that our model excels with single-view inputs and beyond, thus reshaping the paradigm of unsupervised learning in 3D vision. Our contributions signal a substantial leap forward in 3D vision, offering new horizons for content creation across diverse applications. Code is available at https: //github.com/HongbinLin3589/UNeR3D.

1. Introduction

Image-based 3D reconstruction, the process of restoring 3D information from 2D images, has been a key focus in computer vision research, driven by its applications in

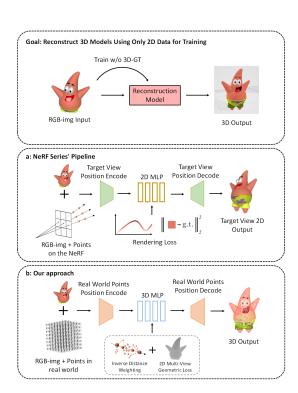


Figure 1. Comparative Overview of 3D Reconstruction. Our goal is to train a model for reconstructing 3D data solely from 2D images. (a) The NeRF series[28, 47, 55, 58] encodes points on the neural radiance field, outputting 2D images of the target camera. (b) Our approach, by encoding average sampled points from the real world and integrating inverse distance weighting with multiview geometric loss, reconstructs realistic 3D models.

diverse fields such as robotics[43], object recognition[12], and medical diagnostics[22]. This transformation from 2D to 3D is crucial for applications where understanding 3D structures from 2D images is vital, including industrial automation and digital avatar creation[15].

Advancements in 2D image processing and computational power have significantly influenced the evolution of

 $^{^{*}}$ Corresponding author. † These authors contributed equally to this work. Preprint. Under review.

3D reconstruction[11, 61]. Traditional methods like Structure from Motion (SfM)[38], Multi-view Stereo (MVS)[7], and Photometric Stereo[14] have utilized multiple images and geometric constraints. The rise of deep learning has further revolutionized this field, enhancing accuracy and complexity handling through volumetric[25, 53], point-based[33], and mesh-based methods[46], along with implicit function representations for complex shape delineation[31, 41].

Despite these advancements, the widespread reliance on 3D Ground Truth data for training models in 3D reconstruction presents significant challenges[5]. Acquiring this data typically requires costly and sophisticated equipment like laser lidars and RGB-D scanners, leading to substantial time and computational costs[6]. After acquisition, extensive processing is necessary to derive usable 3D representations[3, 30, 37]. The relative scarcity of 3D datasets, compared to 2D, hampers the development of 3D reconstruction methods[39], emphasizing the urgent need for innovative, less data-dependent reconstruction techniques.

Neural Radiance Fields (NeRF) and its variants[8, 26, 28, 47, 50, 55, 58] have significantly advanced neural network-based 3D structure representations, improving complex 3D scene rendering. However, they generally lack the ability to generate explicit 3D models, encoding structures implicitly and requiring viewpoint-specific recomputation. The recent focus in generative AI on combining 2D imagery with 3D modeling has led to attempts to integrate NeRF into this domain. Yet, these efforts face challenges like pose alignment due to NeRF's inability to provide direct 3D outputs[17, 21, 23, 40].

Addressing the challenge of developing a generalizable algorithm that relies solely on 2D images for training and produces explicit 3D models, we introduce UNeR3D, an unsupervised 3D reconstruction method infused with 3D prior knowledge. UNeR3D employs ResNet34 for feature extraction and a specialized MLP with point's positional encoding, facilitating the creation of 3D RGB point clouds by combining image data with inverse distance weighting. This method, enhanced by multi-view geometric and color losses, supports various input views, including single-view, for versatile reconstruction. Experimental results demonstrate UNeR3D's superior performance and efficiency in 3D vision, highlighting its potential to transform the field. Our reconstruction approach is poised to tackle a broader range of 3D reconstruction tasks, particularly those requiring alignment of text-to-3D generation.

Our Contributions:

 To the best of our knowledge, UNeR3D is the inaugural model that leverages unsupervised learning to generate high-precision 3D point clouds directly from 2D imagery, substantially reducing the need for labor-

- intensive, supervised training methods.
- We introduce the first method within the NeRF framework capable of reproducing RGB attributes on point clouds, enabling the synthesis of high-fidelity images adaptable to a variable number of input views for enhanced reconstruction flexibility.
- Our approach employs inverse distance weighting for neural rendering, innovatively ensuring smooth color transitions. The trained model can infer point clouds at arbitrary densities, allowing for reconstructions of any desired precision.

2. Related work

2.1. Deep Learning-based 3D Reconstruction

Recent years have seen an upsurge in deep learning techniques dedicated to 3D object reconstruction, prominently structured under voxel-based, mesh-based, and point cloud-based representations. While these methods have garnered impressive results, a common denominator is their reliance on supervised learning paradigms, often necessitating meticulously curated ground truth 3D data for effective training—a significant bottleneck in real-world applicability. Early forays into voxel-based representations used volumetric grids for capturing spatial outlines of objects[4, 9]. Later methods leveraged adaptive octree structures, offering better efficiency and resolution[35, 48], while others integrated context-awareness to bridge single and multi-view reconstructions[49, 54]. Shifting gears to mesh-based reconstructions, frameworks emerged that transformed RGB images directly into 3D mesh structures[32, 46]. The marriage of graphics with deep learning led to realistic surface renderings[20]. The point cloud domain heralded architectures for unordered point set processing[33, 34], and subsequent innovations targeted dense and accurate point cloud reconstructions[24, 45]. Innovations like geometry-aware transformers ushered advancements in point cloud completion tasks[59]. This exposition underscores a poignant lacuna in the field: the quest for a genuine unsupervised learning-based 3D reconstruction method, which we address in this work.

2.2. Positional Encoding and Unsupervised Learning

Positional encoding plays a pivotal role in neural rendering, particularly in enhancing models like NeRF to represent complex spatial details[28]. This technique, which transforms input coordinates for neural networks to capture high-frequency functions better, is instrumental in models' ability to learn detailed geometries, as demonstrated in seminal works such as Vaswani et al.'s[44]. Its application in NeRF highlights its efficacy in achieving detailed 3D scene representations without extensive supervision[42], further

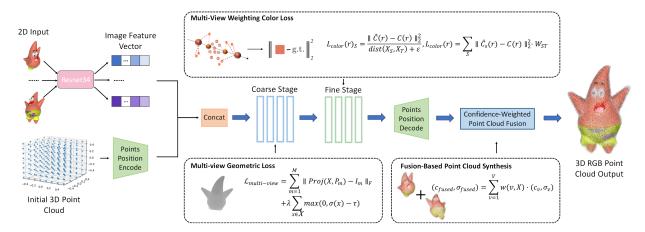


Figure 2. UNeR3D Pipeline: Transforming 2D Images into 3D RGB Point Clouds. The pipeline integrates feature extraction from 2D images, positional encoding of the initial point cloud, and a two-stage neural network processing. In the coarse stage, the Multi-view Geometric Loss shapes the geometric outline of the target object, which is then refined in the fine stage using the Multi-View Weighting Color Loss to endow each point in the point cloud with lifelike colors. The final 3D RGB point cloud is reconstructed by applying confidence weighting.

expanding its utility, non-parametric models like Point-NN leverage non-learnable operations, allowing for sophisticated geometric analysis in point cloud data[60].

Unsupervised 3D reconstruction has evolved through integrating SfM and MVS techniques, essential for deducing spatial depth from imagery [7, 38]. While effective, such methods are traditionally limited by their high computational load and the required extensive array of input views. Groundbreaking efforts, such as Yan et al.'s Perspective Transformer Nets, reduce reliance on 3D ground truth data[56], and Liu et al.'s CAPNet utilizes 2D data to approximate 3D point clouds[29]. However, these techniques still encounter limitations from specific assumptions and prior knowledge needs. Advances in video-based 3D reconstruction by Smith et al. and targeted unsupervised learning for symmetric objects by Jackson et al. showcase the field's progress while highlighting the ongoing need for a flexible and universally applicable unsupervised 3D reconstruction method[13, 16, 52].

2.3. Implicit 3D reconstruction

Implicit representations have redefined the landscape of 3D reconstruction, offering precise surface delineation while minimizing the computational load when contrasted with traditional methods like occupancy grids or voxel frameworks[27]. NeRF stands at the vanguard of this innovation, enabling the generation of volumetric scenes through neural networks, which facilitate photorealistic renderings. PixelNeRF has propelled the adaptability of NeRF by incorporating feature encodings from input images into the MLP, endowing it with the ability to generalize across different scenes[58]. On a parallel front, Point-NeRF[55] merges deep multi-view stereo with NeRF to refine render-

ing, using point clouds to direct the process for enhanced precision and efficiency. Despite its improvements in visual quality, it does not generate point clouds through NeRF's structure and lacks generalizability, fundamentally remaining a 2D rendering model. However, these methods, including advanced variants like NeuS[47], HF-NeuS[50], and NeAT[26], still largely remain within the domain of implicit reconstruction, not directly yielding tangible 3D models from the NeRF framework itself. This limitation has implications for multi-modal alignment in text-to-3D applications, as current NeRF-based methods do not inherently provide a generalizable framework for explicit 3D reconstruction. This gap highlights the need for new approaches to produce usable and adaptable 3D models from 2D inputs directly.

3. Methodology

We present a novel strategy for unsupervised 3D reconstruction from 2D imagery by integrating the neural radiance field concept with a knn-based inverse distance weighting scheme (see Fig. 2). Our method computes the RGB color and confidence of presence for 3D points directly from their coordinates and the associated camera pose of the input image. The reconstruction process consists of querying the RGB color and confidence for each point in the initial point cloud and constructing a refined point cloud that accurately reflects the object's true 3D structure.

The reconstructed point cloud S is formed by aggregating points that surpass a predefined confidence threshold θ :

$$S = \bigcup_{\mathbf{x} \in Q} \{ f(\mathbf{I}, \mathbf{P}, \mathbf{x}) | \alpha(\mathbf{x}) > \theta \}$$
 (1)

Here, Q denotes the initial point cloud, and the function f determines the RGB color and the existence confidence of a point \mathbf{x} within this point cloud. And \mathbf{P} represents the camera pose of the input image \mathbf{I} .

Function f is subsequently defined as:

$$f(\mathbf{I}, \mathbf{P}, \mathbf{x}) = (\mathbf{c}, \alpha) \tag{2}$$

where c represents the predicted RGB color and α signifies the confidence level of the point's existence.

In our framework, the alignment of the generated point cloud with the input imagery is facilitated by a composite loss function:

$$\mathcal{L} = \mathcal{L}_{geom}(S, \mathbf{I}) + \lambda \mathcal{L}_{color}$$
 (3)

Here, \mathcal{L}_{geom} represents the multi-view geometric loss ensuring structural consistency across different views, and \mathcal{L}_{color} enforces color consistency. The parameter λ serves as a balancing coefficient between the two losses.

Subsequent subsections will delve into each component of our methodology, providing a detailed description of the entire pipeline from initial feature extraction to the final 3D structure colorization.

3.1. Initial Point Cloud Generation and Color Discrimination

We initiate our reconstruction process by formulating an initial point cloud X = S(r) from a view-camera pose pair (I, P). The resolution superparameter r governs the granularity of this cubic lattice. This cloud is then transformed from the world to the camera coordinate system using the camera pose P.

Positional encoding of points within **X** leverages sinusoidal functions to facilitate a high-dimensional representation conducive to neural network learning:

$$PosE(p_i) = Concat(sin(\alpha p_i + \beta^{j/C}), cos(\alpha p_i + \beta^{j/C})),$$
$$j \in [0, C/6), \quad (4)$$

where C is a multiple of 6, indicative of the encoding's dimensionality [60].

We employ ResNet-34 to extract feature maps F=E(I) from I. This step is pivotal for the model's generalization across diverse data. Projecting points in X onto F captures view-dependent features, which, alongside positional encodings and the direction vector PosE(d), inform the MLP to predict volume density σ and RGB values rgb:

$$(\sigma, rgb) = N(\pi(F, P, X), PosE(X), PosE(d))$$
 (5)

We construct a 3D representation where points with density σ exceeding the threshold θ (set to zero) are retained

and colored, forming a detailed point cloud of the observed object. Using the source view as the coordinate system stems from our goal to generate a 3D model corresponding to world coordinates, which can be directly transformed into any target view without additional computation. This approach enhances the efficiency and versatility of the reconstruction process, allowing for seamless integration into various application scenarios.

3.2. Coarse-to-Fine Stage Structure

Our methodology employs a coarse-to-fine structure to process the point cloud, enhancing the reconstruction's overall quality by focusing on different objectives at each stage[28, 58]. The specific loss functions utilized in these stages are detailed in Section 3.4.

The coarse stage centers on reconstructing the geometric outline of the target object. Sampling points from the initial point cloud focus on establishing the basic geometric shape, laying a foundation for the detailed reconstruction process. Following the coarse stage, the fine stage refines the details and colors of the model. It processes a denser point cloud sample, concentrating on intricate aspects and color accuracy, which is crucial for the final high-quality 3D model.

This structured approach enables our model to establish the basic shape and structure in the coarse stage and then add detailed refinements in the fine stage, resulting in an effective and high-quality 3D reconstruction.

3.3. Neural Rendering with Inverse Distance Weighting

Considering that actual light behaves not as a singular ray but rather as a viewing cone with a projection area[2], our methodology augments neural radiance rendering by integrating an inverse distance weighting strategy. This approach synthesizes point positions and colors, diverging from the traditional NeRF's 2D rendering limitations. The normalized weighting scheme is critical for supervising the structural and color accuracy of the 3D point cloud, thereby enhancing detail in the reconstructed model.

Figure 3 illustrates our approach where the neural point voxel density-color pair (σ_r, c_r) for each point is calculated by aggregating the k-nearest neighbors within a radius r:

$$(\sigma_r, \mathbf{c}_r) = \left(\frac{\sum_{i=1}^k w_i \sigma_i}{\sum_{i=1}^k w_i + \varepsilon}, \frac{\sum_{i=1}^k w_i \sigma_i c_i}{\sum_{i=1}^k w_i \sigma_i + \varepsilon}\right), \quad (6)$$

The weights w_i are normalized to allow for proportional contributions of neighboring points, calculated as:

$$w_i = \frac{1}{\operatorname{dist}(r, p_i)^2 + \varepsilon},\tag{7}$$

where $\operatorname{dist}(r, p_i)$ is the Euclidean distance between the radiance point r and a point p_i in the point cloud, with ε

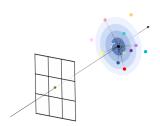


Figure 3. Inverse Distance Weighting in UNeR3D's Rendering for Realistic Coloration. Our approach posits that points further from the neural radiance line influence color rendering less. Our inverse distance weighting captures this, where each point's color impact is inversely related to its distance to the radiance line. This method prioritizes points closer to the object's surface, ensuring a realistic coloration of the point cloud and enhancing the visual authenticity of the reconstructed models.

preventing division by zero. By focusing on points with non-negligible density σ_i , we mitigate the influence of noise points that do not represent the object, ensuring they do not adversely affect the color rendering.

By employing this inverse distance weighting, our rendering protocol guarantees smoother color transitions within a specified neighborhood, avoiding abrupt changes that could disrupt the visual realism. The refinements to the number of points k and the radius r are instrumental in elevating the accuracy and density of the point cloud, significantly contributing to the advancement of unsupervised 3D RGB point cloud reconstruction.

3.4. Loss Function Design

Multi-view Geometric Loss During the coarse stage of training, our model emphasizes the alignment of global structure with the application of a multi-view geometric loss. This loss component is pivotal for establishing the foundational geometry of the reconstructed point cloud across multiple views. By leveraging the geometric adversarial loss (GAL) principles[19], we utilize known camera poses to project the point cloud onto image planes, aligning it with the silhouettes captured in the corresponding images.

With camera pose matrices $\{P_m\}_{m=1}^M$ and corresponding images $\{I_m\}_{m=1}^M$, the geometric loss is computed as:

$$\mathcal{L}_{\text{geom}} = \sum_{m=1}^{M} \| \text{Proj}(\mathbf{X}, \mathbf{P}_m) - \mathbf{I}_m \|_F,$$
 (8)

where $\operatorname{Proj}(\cdot)$ projects points in the point cloud **X** onto the image plane, and $\|\cdot\|_F$ represents the Frobenius norm.

To distinguish points related to the object from background noise, we introduce a regularization term:

$$\mathcal{L}_{\text{reg}} = \lambda \sum_{x \in \mathbf{X}} \max(0, \sigma(x) - \tau), \tag{9}$$

with λ as the regularization weight and τ as the threshold for object relevance.

The coarse stage loss thus combines projection accuracy and regularization:

$$\mathcal{L}_{\text{coarse}} = \mathcal{L}_{\text{geom}} + \mathcal{L}_{\text{reg}}, \tag{10}$$

optimizing for a coherent geometric structure that serves as a scaffold for further refinement in subsequent stages. This multi-view geometric consistency is crucial for the early stages of network training, ensuring the model's global understanding of the 3D structure aligns with the varied perspectives offered by the input views.

Color Consistency with Multi-View Weighting Our color consistency loss function, particularly pertinent during the fine stage of our model's training, integrates multi-view considerations to ensure accurate color reproduction. The loss for a ray r, formulated as follows, weighs the contributions from various source views against the target view utilized during the supervised training phase:

$$\mathcal{L}_{\text{color}}(r)_S = \frac{\|\hat{c}(r) - C(r)\|_2^2}{\text{dist}(X_S, X_T) + \varepsilon},\tag{11}$$

where $\hat{c}(r)$ represents the estimated color along ray r, C(r) is the actual color from the ground truth, and $\mathrm{dist}(X_S, X_T)$ is the distance between the source view X_S and the target view X_T used for training supervision. The addition of a small constant ε prevents division by zero.

The aggregated color loss across all views is then given by:

$$\mathcal{L}_{\text{fine}} = \mathcal{L}_{\text{color}}(r) = \sum_{S} \|\hat{C}_s(r) - C(r)\|_2^2 \cdot W_{ST}, \quad (12)$$

with the view weighting factor W_{ST} normalized across all source views S relative to the target view T:

$$W_{ST} = \frac{\frac{1}{\operatorname{dist}(x_S, x_T) + \varepsilon}}{\sum_S \frac{1}{\operatorname{dist}(x_S, x_T) + \varepsilon}}.$$
 (13)

This loss function ensures that the computed colors are consistent with the observed ones, effectively training the model to render accurate and coherent images across multiple viewpoints.

3.5. Fusion-Based Point Cloud Synthesis

Our model's architecture is adept at handling a flexible number of views for reconstruction, from a single view to multiple views. This flexibility is achieved through a unified weighting scheme that adapts to the available input views for single-view or multi-view reconstructions.

The synthesis of the point cloud is directed by an equation that uniformly accounts for the contribution of each view:

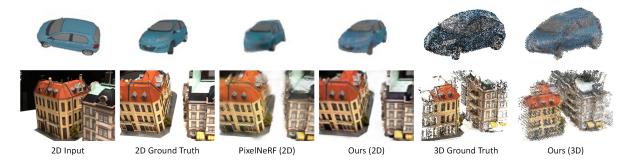


Figure 4. Comparative Generalization Performance on Unseen Images from ShapeNet and DTU Datasets: A side-by-side comparison between UNeR3D and PixelNeRF demonstrates the enhanced clarity and detail resolution achieved by our method, underlining its superior ability in generalizing to unseen images with greater visual fidelity.

$$(c_{\text{fused}}, \sigma_{\text{fused}}) = \sum_{v=1}^{V} w(v, X) \cdot (c_v, \sigma_v), \qquad (14)$$

Here, V denotes the number of views available for reconstruction (V=1 signifies a single-view), X represents a point within the point cloud, and w(v,X) is the calculated weight for view v at point X. The weights are derived by combining a distance-based factor and the transmittance along the ray from each view:

$$w(v, X) = \frac{W_k(v, X)}{\max\{W_k(v, X)\}} \exp\left(-\int_{s_n}^s \sigma(\mathbf{r}_v(s)) \, ds\right),$$
(15)

where $W_k(v,X)$ is the distance-based weight for view v and point X, as defined by Equation 7. This normalization ensures that each view's contribution is proportionally adjusted based on its distance to the neural radiance point, with closer views having a more significant influence on the final point cloud.

Our method enables reconstruction from any number of views post-training, including a single image, but also facilitates the derivation of point clouds at any desired density, allowing for reconstructions of varying precision that cater to different resolution requirements without additional training. The synthesis process, which adaptively weights the contributions of each view, accentuates the model's versatility by leveraging the MLP's learned priors along with the geometric and photometric data from input views, enabling the generation of detailed and precise 3D point clouds, showcasing our model's ability to integrate and adaptively apply comprehensive learned information to a wide range of reconstruction scenarios.

4. Experiments

In this section, we present a comprehensive evaluation of our model, contrasting it against state-of-the-art NeRF variants including PixelNeRF[58], PointNeRF[55], and NeuS[47], using the ShapeNet[53] and DTU[1] datasets. Furthermore, we conduct a series of ablation studies to dissect the contributions of each component within our framework, substantiating the superiority of our proposed model.

4.1. Datasets

Shapenet ShapeNet is an extensive collection of 3D objects with rich annotations[53]. It covers a diverse set of categories, including furniture, vehicles, and electronics, among others, amounting to over 50,000 unique 3D models. Each category comprises a substantial number of examples, which supports training robust models capable of generalizing across various shapes and structures.

DTU The DTU dataset, on the other hand, is a photogrammetric dataset containing images of intricate 3D scenes, designed specifically for 3D reconstruction tasks[1]. It provides high-resolution images and accurate 3D surface models, contributing to a total of several scenes with different textures, geometries, and lighting conditions.

4.2. Experimental Setup

Implementation Details In our implementation, the camera's rotation coordinates were set within a spherical coordinate system, with the longitude and latitude angles ranging from 0 to 2π , allowing for complete environmental capture. The camera's translation coordinates, and the point cloud coordinate system were defined in a three-dimensional Cartesian coordinate system. To facilitate calculations and maintain consistency, the range for the point cloud Cartesian coordinates was normalized to [-1, 1] across all three axes. Our training protocol included different numbers of views per object—2, 4, and 8—to investigate the impact of view count on the model's ability to assimilate and generalize prior knowledge. The division of our datasets into training, validation, and test sets adhered to a 7:2:1 ratio. ensuring a thorough assessment across various sections of the data.

Table 1. Performance Comparison on ShapeNet and DTU datasets

Metric	UNeR3D (Ours)	PixelNeRF[58]	PointNeRF[55]	NeUS[47]
2D SSIM↑ (Generalization) - ShapeNet	0.957	0.918	-	-
2D SSIM↑ (Generalization) - DTU	0.908	0.823	-	-
2D PSNR↑ (Generalization) - ShapeNet	28.413	22.783	-	-
2D PSNR↑ (Generalization) - DTU	25.617	16.634	-	-
2D PSNR↑ (Single Scene) - DTU	28.468	=	21.367	30.851
2D SSIM↑ (Single Scene) - DTU	0.873	=	0.818	0.931
3D EMD↓ (Single Scene) - DTU	0.362	=	0.672	0.813

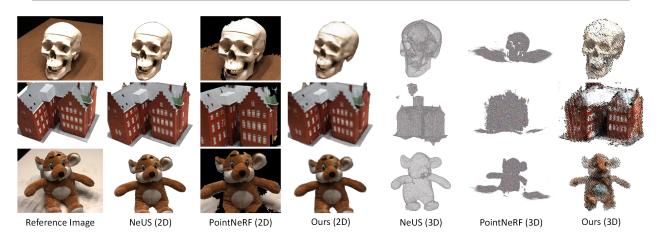


Figure 5. Comparison of 2D and 3D reconstruction outcomes on a single scene from the DTU dataset: UNeR3D versus PointNeRF and NeUS. Our approach, with its unique capability to restore color in 3D reconstruction, achieves more lifelike and visually compelling 3D results.

Evaluation Metrics We employed the PSNR and SSIM[51] for RGB image fidelity, and the Earth Mover's Distance (EMD)[36] to assess 3D point cloud reconstruction, comparing all against ground truth data. Notably, our model's training did not involve 3D data, with 3D GT only used for post-training evaluation to confirm the model's 3D inference accuracy. Notably, during training, our model was not exposed to any 3D information. The utilization of 3D GT data was strictly confined to the performance evaluation stage, ensuring an unbiased validation of the model's capability to infer 3D structures. This approach underlines the effectiveness of our model in learning from 2D data while being capable of accurate 3D predictions, a key aspect of our experimental validation.

4.3. Comparisons

Baseline In this section, we benchmark our UNeR3D model against prominent NeRF variants, namely PixelNeRF[58], PointNeRF[55], and NeUS[47]. PixelNeRF is notable for its ability to generate 2D images from novel viewpoints using 2D images as input, showcasing significant generalization capabilities. PointNeRF leverages MVS-generated

point clouds[57] to guide NeRF for refined rendering, though it lacks 3D output capabilities. NeUS excels in producing detailed 3D models through extensive iterations over a single scene but needs more generalizability. Table 2 delineates the performance comparison across various dimensions: 2D output, 3D output, 3D RGB attributes, generalization abilities, and number of training iterations, highlighting the comprehensive superiority of our approach.

Table 2. Comparative Results between UNeR3D (Ours) and Baseline Models

Comparison	Ours	Pixel-	Point-	NeUS
Aspect		NeRF	NeRF	
2D Output	√	√	√	√
3D Output	\checkmark	-	\checkmark	\checkmark
3D RGB Attributes	\checkmark	-	-	-
Generalizability	\checkmark	\checkmark	-	-

Note: The 3D output for PointNeRF is derived from MVS[57], not directly from the NeRF pipeline, while UNeR3D's is integrated within the NeRF pipeline.

Qualitative Results Figure 4 and 5 presents a visual comparison of our UNeR3D model against the baseline models

mentioned previously: PixelNeRF, PointNeRF, and NeUS. Visually, our model generates three-dimensional reconstructions with superior clarity and detail. In terms of two-dimensional imagery, our results are comparable and, in some aspects, indistinguishable from those generated by the baselines, highlighting the robustness of our approach while maintaining high fidelity in 3D structure generation.

Quantitative Results We conducted training and evaluation on identical datasets and splits for our UNeR3D model and the comparison models to assess generalization capabilities. Specifically, UNeR3D demonstrated superior performance in single-scene training scenarios, achieving results comparable to NeUS with significantly fewer iterations. Our model reached a performance level similar to NeUS's 150,000 iterations at around 30,000 iterations. However, as NeUS continually converges with more iterations due to its non-generalizable nature, UNeR3D's precision plateaus beyond a certain iteration count, reflecting its inherent generalizability. Detailed quantitative outcomes are illustrated in Table 1.

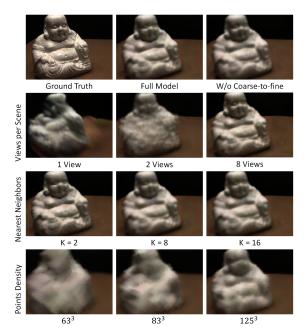


Figure 6. Comparative visualization of the ablation study results.

4.4. Ablation Study

To discern the influence of individual components within our model, we conducted an ablation study focusing on the coarse-to-fine network, the number of views per object per epoch during training, the number of nearest neighbors in the inverse distance weighting, and the initial point cloud density. We evaluated each variation on the DTU dataset, with performance measured by PSNR, SSIM, and EMD metrics. The detailed results are tabulated in Table 3. Vi-

sual results of the ablation study are illustrated in Figure 11, and a thorough analysis with additional visualizations and discussions is included in the Appendix.

Table 3. Ablation study results on the ShapeNet dataset, showcasing the influence of different model configurations on the PSNR, SSIM, and EMD metrics.

Configuration	PSNR↑	SSIM↑	EMD↓
Baseline (Full Model)	25.617	0.908	0.362
w/o Coarse-to-Fine	25.282	0.899	0.0397
Views per Scene: 1	16.992	0.585	1.15
Views per Scene: 2	20.325	0.703	1.10
Views per Scene: 3	23.729	0.798	0.664
Nearest Neighbors: 2	24.806	0.931	0.388
Nearest Neighbors: 8	25.004	0.885	0.415
Nearest Neighbors: 16	25.272	0.905	0.401
Point Cloud Density: 63 ³	19.335	0.717	0.102
Point Cloud Density: 83 ³	19.545	0.725	0.099
Point Cloud Density: 125 ³	22.137	0.804	0.687

5. Limitations and Conclusion

Limitations Despite achieving promising results, UNeR3D faces certain limitations. Our generated 2D views still exhibit artifacts due to the model's generalizability. Furthermore, in complex scenes, the distinction between foreground and background elements can become blurred, affecting the clarity of scene structure.

Conclusion Our study presents UNeR3D as an innovative approach to unsupervised 3D reconstruction, effectively bypassing the need for 3D ground truth data throughout the training process. By solely utilizing 2D images, our model achieves the generation of high-fidelity 3D RGB point clouds. This achievement aligns with advances in generative AI and the shift towards creating 3D content directly from textual and 2D visual inputs. Our framework's flexibility, allowing for reconstructions from an arbitrary number of views, including single-view inputs post-training, significantly lowers the threshold for engaging in 3D reconstruction tasks and democratizes the process. As we progress in the era of generative content creation, UNeR3D holds the promise of revolutionizing 3D modeling and rendering, bridging the gap between 2D imagery and 3D digital objects. Its implications could enrich multiple fields, from virtual reality environments to robotic perception[10, 18]. Our work lays a new foundation for unsupervised learning in 3D vision. It opens up exciting avenues for future research and applications in the rapidly evolving landscape of AI-driven content generation.

6. Acknowledgement

This work is supported by the National Natural Science Foundation of China under Grant 52175237 and the National Key Research and Development Program of China under Grant 2022YFB4703000.

References

- [1] Henrik Aanæs, Rasmus Ramsbøl Jensen, George Vogiatzis, Engin Tola, and Anders Bjorholm Dahl. Large-scale data for multiple-view stereopsis. *International Journal of Computer Vision*, 120:153–168, 2016. 6, 2
- [2] Jonathan T Barron, Ben Mildenhall, Matthew Tancik, Peter Hedman, Ricardo Martin-Brualla, and Pratul P Srinivasan. Mip-nerf: A multiscale representation for anti-aliasing neural radiance fields. In *Proceedings of the IEEE/CVF International Conference on Computer Vision*, pages 5855–5864, 2021. 4
- [3] Matthew Berger, Andrea Tagliasacchi, Lee M Seversky, Pierre Alliez, Gael Guennebaud, Joshua A Levine, Andrei Sharf, and Claudio T Silva. A survey of surface reconstruction from point clouds. In *Computer graphics forum*, pages 301–329. Wiley Online Library, 2017. 2
- [4] Christopher B Choy, Danfei Xu, Jun Young Gwak, Kevin Chen, and Silvio Savarese. 3d-r2n2: A unified approach for single and multi-view 3d object reconstruction. In Computer Vision–ECCV 2016: 14th European Conference, Amsterdam, The Netherlands, October 11-14, 2016, Proceedings, Part VIII 14, pages 628–644. Springer, 2016. 2
- [5] Angela Dai, Charles Ruizhongtai Qi, and Matthias Nießner. Shape completion using 3d-encoder-predictor cnns and shape synthesis. In *Proceedings of the IEEE conference on computer vision and pattern recognition*, pages 5868–5877, 2017. 2
- [6] Mingsong Dou, Sameh Khamis, Yury Degtyarev, Philip Davidson, Sean Ryan Fanello, Adarsh Kowdle, Sergio Orts Escolano, Christoph Rhemann, David Kim, Jonathan Taylor, et al. Fusion4d: Real-time performance capture of challenging scenes. ACM Transactions on Graphics (ToG), 35(4): 1–13, 2016.
- [7] Yasutaka Furukawa, Carlos Hernández, et al. Multi-view stereo: A tutorial. *Foundations and Trends*® *in Computer Graphics and Vision*, 9(1-2):1–148, 2015. 2, 3
- [8] Wenhang Ge, Tao Hu, Haoyu Zhao, Shu Liu, and Ying-Cong Chen. Ref-neus: Ambiguity-reduced neural implicit surface learning for multi-view reconstruction with reflection. *arXiv* preprint arXiv:2303.10840, 2023. 2
- [9] Rohit Girdhar, David F Fouhey, Mikel Rodriguez, and Abhinav Gupta. Learning a predictable and generative vector representation for objects. In Computer Vision–ECCV 2016: 14th European Conference, Amsterdam, The Netherlands, October 11-14, 2016, Proceedings, Part VI 14, pages 484–499. Springer, 2016. 2
- [10] Hyun Woo Goo, Sang Joon Park, and Shi-Joon Yoo. Advanced medical use of three-dimensional imaging in congenital heart disease: augmented reality, mixed reality, virtual

- reality, and three-dimensional printing. *Korean journal of radiology*, 21(2):133–145, 2020. 8
- [11] Xian-Feng Han, Hamid Laga, and Mohammed Bennamoun. Image-based 3d object reconstruction: State-of-the-art and trends in the deep learning era. *IEEE transactions on pattern* analysis and machine intelligence, 43(5):1578–1604, 2019.
- [12] Kaiming He, Xiangyu Zhang, Shaoqing Ren, and Jian Sun. Deep residual learning for image recognition. In *Proceedings of the IEEE conference on computer vision and pattern recognition*, pages 770–778, 2016. 1
- [13] Philipp Henzler, Jeremy Reizenstein, Patrick Labatut, Roman Shapovalov, Tobias Ritschel, Andrea Vedaldi, and David Novotny. Unsupervised learning of 3d object categories from videos in the wild. In *Proceedings of the IEEE/CVF Conference on Computer Vision and Pattern Recognition*, pages 4700–4709, 2021. 3
- [14] Steffen Herbort and Christian Wöhler. An introduction to image-based 3d surface reconstruction and a survey of photometric stereo methods. *3D Research*, 2(3):1–17, 2011. 2
- [15] Fangzhou Hong, Mingyuan Zhang, Liang Pan, Zhongang Cai, Lei Yang, and Ziwei Liu. Avatarclip: Zero-shot textdriven generation and animation of 3d avatars. arXiv preprint arXiv:2205.08535, 2022.
- [16] Zhengyu Hu, Jieyu Zhang, Haonan Wang, Siwei Liu, and Shangsong Liang. Leveraging relational graph neural network for transductive model ensemble. In *Proceedings of* the 29th ACM SIGKDD Conference on Knowledge Discovery and Data Mining, pages 775–787, 2023. 3
- [17] Ajay Jain, Ben Mildenhall, Jonathan T Barron, Pieter Abbeel, and Ben Poole. Zero-shot text-guided object generation with dream fields. In *Proceedings of the IEEE/CVF Con*ference on Computer Vision and Pattern Recognition, pages 867–876, 2022. 2
- [18] Jiaqi Jiang, Guanqun Cao, Jiankang Deng, Thanh-Toan Do, and Shan Luo. Robotic perception of transparent objects: A review. *IEEE Transactions on Artificial Intelligence*, 2023.
- [19] Li Jiang, Shaoshuai Shi, Xiaojuan Qi, and Jiaya Jia. Gal: Geometric adversarial loss for single-view 3d-object reconstruction. In *Proceedings of the European conference on computer vision (ECCV)*, pages 802–816, 2018. 5
- [20] Hiroharu Kato, Yoshitaka Ushiku, and Tatsuya Harada. Neural 3d mesh renderer. In Proceedings of the IEEE conference on computer vision and pattern recognition, pages 3907–3916, 2018.
- [21] Leheng Li, Qing Lian, and Ying-Cong Chen. Adv3d: Generating 3d adversarial examples in driving scenarios with nerf. arXiv preprint arXiv:2309.01351, 2023. 2
- [22] Geert Litjens, Thijs Kooi, Babak Ehteshami Bejnordi, Arnaud Arindra Adiyoso Setio, Francesco Ciompi, Mohsen Ghafoorian, Jeroen Awm Van Der Laak, Bram Van Ginneken, and Clara I Sánchez. A survey on deep learning in medical image analysis. *Medical image analysis*, 42:60–88, 2017.
- [23] Minghua Liu, Chao Xu, Haian Jin, Linghao Chen, Zexiang Xu, Hao Su, et al. One-2-3-45: Any single image to 3d mesh

- in 45 seconds without per-shape optimization. *arXiv preprint* arXiv:2306.16928, 2023. 2
- [24] Priyanka Mandikal and Venkatesh Babu Radhakrishnan. Dense 3d point cloud reconstruction using a deep pyramid network. In 2019 IEEE Winter Conference on Applications of Computer Vision (WACV), pages 1052–1060. IEEE, 2019.
- [25] Daniel Maturana and Sebastian Scherer. Voxnet: A 3d convolutional neural network for real-time object recognition. In 2015 IEEE/RSJ international conference on intelligent robots and systems (IROS), pages 922–928. IEEE, 2015. 2
- [26] Xiaoxu Meng, Weikai Chen, and Bo Yang. Neat: Learning neural implicit surfaces with arbitrary topologies from multi-view images. In *Proceedings of the IEEE/CVF Conference on Computer Vision and Pattern Recognition*, pages 248–258, 2023. 2, 3
- [27] Lars Mescheder, Michael Oechsle, Michael Niemeyer, Sebastian Nowozin, and Andreas Geiger. Occupancy networks: Learning 3d reconstruction in function space. In *Proceedings of the IEEE/CVF conference on computer vision and pattern recognition*, pages 4460–4470, 2019. 3
- [28] Ben Mildenhall, Pratul P Srinivasan, Matthew Tancik, Jonathan T Barron, Ravi Ramamoorthi, and Ren Ng. Nerf: Representing scenes as neural radiance fields for view synthesis. *Communications of the ACM*, 65(1):99–106, 2021. 1, 2, 4
- [29] KL Navaneet, Priyanka Mandikal, Mayank Agarwal, and R Venkatesh Babu. Capnet: Continuous approximation projection for 3d point cloud reconstruction using 2d supervision. In *Proceedings of the AAAI Conference on Artificial Intelligence*, pages 8819–8826, 2019. 3
- [30] Richard A Newcombe, Shahram Izadi, Otmar Hilliges, David Molyneaux, David Kim, Andrew J Davison, Pushmeet Kohi, Jamie Shotton, Steve Hodges, and Andrew Fitzgibbon. Kinectfusion: Real-time dense surface mapping and tracking. In 2011 10th IEEE international symposium on mixed and augmented reality, pages 127–136. Ieee, 2011. 2
- [31] Jeong Joon Park, Peter Florence, Julian Straub, Richard Newcombe, and Steven Lovegrove. Deepsdf: Learning continuous signed distance functions for shape representation. In *Proceedings of the IEEE/CVF conference on computer vision and pattern recognition*, pages 165–174, 2019. 2
- [32] Jhony K Pontes, Chen Kong, Sridha Sridharan, Simon Lucey, Anders Eriksson, and Clinton Fookes. Image2mesh: A learning framework for single image 3d reconstruction. In Computer Vision—ACCV 2018: 14th Asian Conference on Computer Vision, Perth, Australia, December 2–6, 2018, Revised Selected Papers, Part I 14, pages 365–381. Springer, 2019. 2
- [33] Charles R Qi, Hao Su, Kaichun Mo, and Leonidas J Guibas. Pointnet: Deep learning on point sets for 3d classification and segmentation. In *Proceedings of the IEEE conference* on computer vision and pattern recognition, pages 652–660, 2017.
- [34] Charles Ruizhongtai Qi, Li Yi, Hao Su, and Leonidas J Guibas. Pointnet++: Deep hierarchical feature learning on point sets in a metric space. *Advances in neural information processing systems*, 30, 2017. 2

- [35] Gernot Riegler, Ali Osman Ulusoy, and Andreas Geiger. Octnet: Learning deep 3d representations at high resolutions. In Proceedings of the IEEE conference on computer vision and pattern recognition, pages 3577–3586, 2017.
- [36] Yossi Rubner, Carlo Tomasi, and Leonidas J Guibas. The earth mover's distance as a metric for image retrieval. *International journal of computer vision*, 40:99–121, 2000. 7
- [37] Szymon Rusinkiewicz and Marc Levoy. Efficient variants of the icp algorithm. In *Proceedings third international conference on 3-D digital imaging and modeling*, pages 145–152. IEEE, 2001. 2
- [38] Johannes L Schonberger and Jan-Michael Frahm. Structurefrom-motion revisited. In *Proceedings of the IEEE conference on computer vision and pattern recognition*, pages 4104–4113, 2016. 2, 3
- [39] Nathan Silberman, Derek Hoiem, Pushmeet Kohli, and Rob Fergus. Indoor segmentation and support inference from rgbd images. In Computer Vision–ECCV 2012: 12th European Conference on Computer Vision, Florence, Italy, October 7-13, 2012, Proceedings, Part V 12, pages 746–760. Springer, 2012. 2
- [40] Uriel Singer, Shelly Sheynin, Adam Polyak, Oron Ashual, Iurii Makarov, Filippos Kokkinos, Naman Goyal, Andrea Vedaldi, Devi Parikh, Justin Johnson, et al. Text-to-4d dynamic scene generation. arXiv preprint arXiv:2301.11280, 2023. 2
- [41] Vincent Sitzmann, Michael Zollhöfer, and Gordon Wetzstein. Scene representation networks: Continuous 3d-structure-aware neural scene representations. *Advances in Neural Information Processing Systems*, 32, 2019. 2
- [42] Matthew Tancik, Pratul Srinivasan, Ben Mildenhall, Sara Fridovich-Keil, Nithin Raghavan, Utkarsh Singhal, Ravi Ramamoorthi, Jonathan Barron, and Ren Ng. Fourier features let networks learn high frequency functions in low dimensional domains. Advances in Neural Information Processing Systems, 33:7537–7547, 2020. 2
- [43] Sebastian Thrun. Probabilistic robotics. Communications of the ACM, 45(3):52–57, 2002.
- [44] Ashish Vaswani, Noam Shazeer, Niki Parmar, Jakob Uszkoreit, Llion Jones, Aidan N Gomez, Łukasz Kaiser, and Illia Polosukhin. Attention is all you need. Advances in neural information processing systems, 30, 2017.
- [45] Jinglu Wang, Bo Sun, and Yan Lu. Mvpnet: Multi-view point regression networks for 3d object reconstruction from a single image. In *Proceedings of the AAAI Conference on Artificial Intelligence*, pages 8949–8956, 2019.
- [46] Nanyang Wang, Yinda Zhang, Zhuwen Li, Yanwei Fu, Wei Liu, and Yu-Gang Jiang. Pixel2mesh: Generating 3d mesh models from single rgb images. In *Proceedings of the European conference on computer vision (ECCV)*, pages 52–67, 2018.
- [47] Peng Wang, Lingjie Liu, Yuan Liu, Christian Theobalt, Taku Komura, and Wenping Wang. Neus: Learning neural implicit surfaces by volume rendering for multi-view reconstruction. *arXiv preprint arXiv:2106.10689*, 2021. 1, 2, 3, 6, 7
- [48] Peng-Shuai Wang, Chun-Yu Sun, Yang Liu, and Xin Tong. Adaptive o-cnn: A patch-based deep representation of 3d

- shapes. ACM Transactions on Graphics (TOG), 37(6):1–11, 2018. 2
- [49] Weiyue Wang, Qiangui Huang, Suya You, Chao Yang, and Ulrich Neumann. Shape inpainting using 3d generative adversarial network and recurrent convolutional networks. In *Proceedings of the IEEE international conference on computer vision*, pages 2298–2306, 2017. 2
- [50] Yiqun Wang, Ivan Skorokhodov, and Peter Wonka. Hf-neus: Improved surface reconstruction using high-frequency details. Advances in Neural Information Processing Systems, 35:1966–1978, 2022. 2, 3
- [51] Zhou Wang, Alan C Bovik, Hamid R Sheikh, and Eero P Simoncelli. Image quality assessment: from error visibility to structural similarity. *IEEE transactions on image processing*, 13(4):600–612, 2004. 7
- [52] Shangzhe Wu, Christian Rupprecht, and Andrea Vedaldi. Unsupervised learning of probably symmetric deformable 3d objects from images in the wild. In *Proceedings of the IEEE/CVF conference on computer vision and pattern recognition*, pages 1–10, 2020. 3
- [53] Zhirong Wu, Shuran Song, Aditya Khosla, Fisher Yu, Linguang Zhang, Xiaoou Tang, and Jianxiong Xiao. 3d shapenets: A deep representation for volumetric shapes. In Proceedings of the IEEE conference on computer vision and pattern recognition, pages 1912–1920, 2015. 2, 6
- [54] Haozhe Xie, Hongxun Yao, Xiaoshuai Sun, Shangchen Zhou, and Shengping Zhang. Pix2vox: Context-aware 3d reconstruction from single and multi-view images. In *Pro*ceedings of the IEEE/CVF international conference on computer vision, pages 2690–2698, 2019. 2
- [55] Qiangeng Xu, Zexiang Xu, Julien Philip, Sai Bi, Zhixin Shu, Kalyan Sunkavalli, and Ulrich Neumann. Point-nerf: Point-based neural radiance fields. In *Proceedings of the IEEE/CVF Conference on Computer Vision and Pattern Recognition*, pages 5438–5448, 2022. 1, 2, 3, 6, 7
- [56] Xinchen Yan, Jimei Yang, Ersin Yumer, Yijie Guo, and Honglak Lee. Perspective transformer nets: Learning singleview 3d object reconstruction without 3d supervision. Advances in neural information processing systems, 29, 2016.
- [57] Yao Yao, Zixin Luo, Shiwei Li, Tian Fang, and Long Quan. Mvsnet: Depth inference for unstructured multi-view stereo. In *Proceedings of the European conference on computer vision (ECCV)*, pages 767–783, 2018.
- [58] Alex Yu, Vickie Ye, Matthew Tancik, and Angjoo Kanazawa. pixelnerf: Neural radiance fields from one or few images. In *Proceedings of the IEEE/CVF Conference on Computer Vision and Pattern Recognition*, pages 4578–4587, 2021. 1, 2, 3, 4, 6, 7
- [59] Xumin Yu, Yongming Rao, Ziyi Wang, Zuyan Liu, Jiwen Lu, and Jie Zhou. Pointr: Diverse point cloud completion with geometry-aware transformers. In *Proceedings of the IEEE/CVF international conference on computer vision*, pages 12498–12507, 2021. 2
- [60] Renrui Zhang, Liuhui Wang, Yali Wang, Peng Gao, Hong-sheng Li, and Jianbo Shi. Parameter is not all you need: Starting from non-parametric networks for 3d point cloud analysis. arXiv preprint arXiv:2303.08134, 2023. 3, 4

[61] Fang Zhu, Shuai Guo, Li Song, Ke Xu, Jiayu Hu, et al. Deep review and analysis of recent nerfs. APSIPA Transactions on Signal and Information Processing, 12(1), 2023.

UNeR3D: Versatile and Scalable 3D RGB Point Cloud Generation from 2D Images in Unsupervised Reconstruction

Supplementary Material

7. Additional Experimental Results

This appendix section delves into comprehensive experimental analyses and additional results that extend beyond the scope of the main paper. These supplementary experiments aim to validate further the robustness and generalizability of our UNeR3D model across diverse datasets and real-world scenarios.

7.1. Generalization on ShapeNet Subsets and DTU Dataset

To rigorously evaluate the generalization capabilities of our UNeR3D model, we extended our experiments to include four diverse subsets from the ShapeNet dataset: chairs, cars, lamps, and planes. These subsets were selected for their varying geometric shapes and textural complexities, posing a broad spectrum of challenges ideal for benchmarking our model's performance in an unsupervised setting. The results, depicted in Figure 8, highlight our model's adeptness in adapting to different object categories. This demonstrates UNeR3D's robustness in processing various 3D structures and reinforces its potential in versatile real-world applications. Furthermore, our model exhibited strong generalization performance on the DTU dataset, where PixelNeRF typically shows limitations. This underscores the enhanced adaptability of UNeR3D to various real-world scenarios. The visuals demonstrating this superior performance are presented in Figure 9. Additionally, our ablation study, results of which are showcased in Figure 11, confirms the impact of each module on the model's performance, underscoring the effectiveness of our model design.

7.2. Real-world Data Validation

In addition to standard datasets, we sought to challenge our model with real-world data, often presenting a higher degree of complexity and variability. To this end, we curated a collection of intricate models from the internet, including cartoon characters and abstract objects like 'Patrick Star' from popular media. These models, characterized by their non-standard shapes and unique textural patterns, were used to evaluate how well our model performs under real-world conditions. As depicted in Figure 10, the results demonstrate our model's effectiveness in rendering realistic and coherent 3D reconstructions from diverse and complex real-world data sources.

These additional experiments underscore the versatility of UNeR3D, highlighting its potential for wide-ranging

applications in 3D vision and beyond. Our findings corroborate the model's ability to generalize across different datasets, maintain high precision in detail-rich reconstructions, and adapt effectively to real-world data challenges.

8. Network Architectures and Parameters

In our UNeR3D model, we employed a carefully designed Multi-Layer Perceptron (MLP) architecture, optimized for efficient and accurate 3D reconstruction from 2D imagery. The MLP structure, detailed in Figure 7, is built to effectively process positional encodings and image feature vectors, crucial for predicting volumetric density and RGB values of the point cloud.

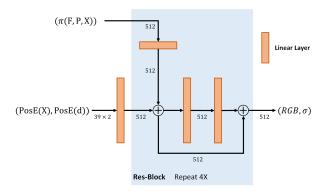


Figure 7. Our MLP structure, composed of four Res-Blocks, takes as input the positionally encoded real-world points ($\operatorname{PosE}(X),\operatorname{PosE}(d)$) and the feature-extracted image ($\pi(F,P,X)$). This design facilitates the integration of spatial and visual data, crucial for generating high-fidelity 3D RGB point clouds.

The entire model was developed using the PyTorch framework and trained on a single Nvidia A800 GPU. This setup was chosen to strike a balance between computational power and efficiency, catering to the resource-intensive nature of our reconstruction tasks. For optimization, we utilized the Adam optimizer, with a learning rate set at 1×10^{-4} and no decay over epochs, ensuring steady progression in learning.

During training, we maintained a batch size of 1 to optimize memory usage and computational performance on the GPU. For each input image, the model generates 256 neural radiance lines, a parameter that balances the need for detailed reconstruction against computational constraints. This configuration allows our model to process a

wide range of images, achieving high-precision 3D reconstruction while ensuring efficient use of computational resources.

9. Dataset Details

In our experimental setup, we utilized three distinct datasets: ShapeNet[53], DTU[1], and real-world data, each presenting unique characteristics and challenges.

ShapeNet and DTU Datasets: For both ShapeNet and DTU datasets, camera extrinsics were predetermined to obtain the camera pose matrices, crucial for our model's training and evaluation. In the case of the DTU dataset, inspired by the methodology of NeUS[47], we employed masks to enhance training effectiveness. These masks help isolate the object of interest from complex backgrounds, thereby focusing the model's learning on relevant features.

Real-world Data Collection: The real-world data, essential for testing our model's generalization capabilities, were sourced from Sketchfab¹. We specifically selected free-to-use models from this platform, ensuring that the data were used solely for experimental and research purposes, with no commercial intent. The inclusion of these real-world models provides a rigorous testbed for our algorithm, challenging it with data that closely mimics the diversity and complexity encountered in natural environments.

This diverse dataset compilation allowed us to thoroughly evaluate our model across various scenarios, ensuring its robustness and adaptability to both synthetic and real-world conditions.

10. Future Work Directions

Our research with UNeR3D has opened multiple avenues for future exploration and development in 3D reconstruction. We envision the following key areas as vital for advancing our work:

Integration with 3D Generative Models: A promising direction is the amalgamation of our model with 3D generative models, particularly those based on the NeRF framework currently prevalent in text-to-3D research. The implicit nature of NeRF's reconstructions presents challenges in central alignment, an issue that can be potentially mitigated by incorporating our explicit 3D model outputs. This integration could optimize multi-modal alignment processes, enhancing the central alignment and overall fidelity of generated 3D models.

Refinement of 3D Output Quality: While our model successfully outputs 3D RGB point clouds, there are scenarios where it produces noise, particularly black dots, mainly due to suboptimal separation from the background. Future efforts could focus on refining these outputs, striving for higher quality and resolution. This could involve integrating

advanced texture sculpting techniques to elevate the visual quality of the reconstructed models, pushing the boundaries of 3D rendering realism.

Camera Pose Independence: Our current model still relies on input camera pose matrices. A significant leap would be to unlock the constraints of camera pose, allowing for the input of images from arbitrary angles without needing registration. This development would free the reconstruction process from the limitations of shooting angles, broaden the range of practical applications, and make the technology more accessible and versatile for various real-world scenarios.

These future directions not only aim to enhance the capabilities of our current model but also signify a broader impact on the field of 3D vision, potentially revolutionizing how we approach 3D content creation from 2D data sources.

https://sketchfab.com/3d-models

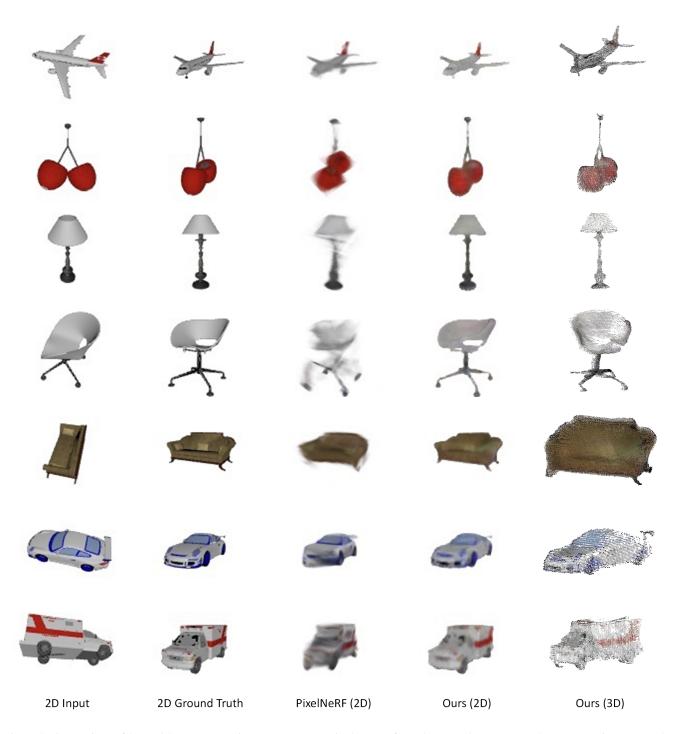


Figure 8. Comparison of 2D and 3D reconstruction outcomes on a single scene from the DTU dataset: UNeR3D versus PointNeRF and NeUS. Our approach, with its unique capability to restore color in 3D reconstruction, achieves more lifelike and visually compelling 3D results.

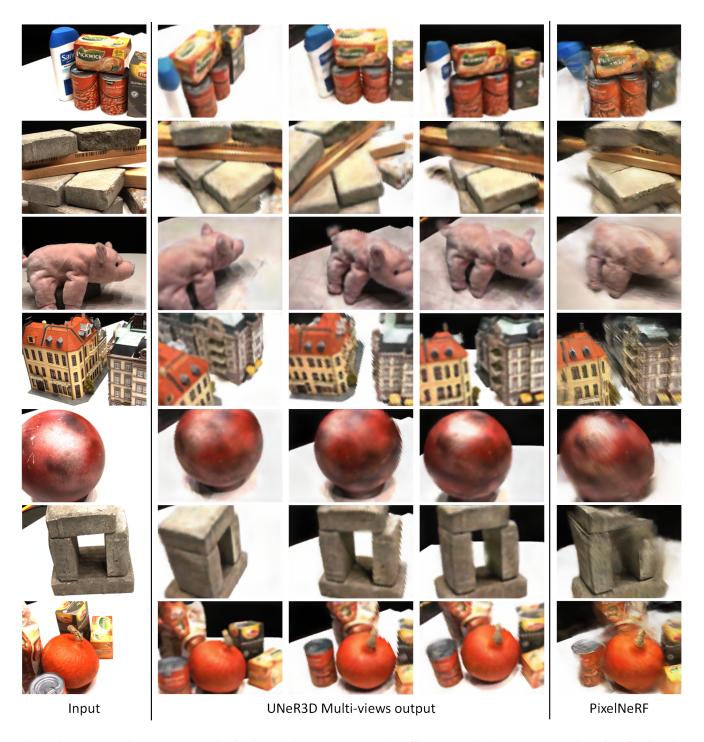


Figure 9. Demonstrating robust generalization in complex scenes, our model effectively maintains the structural integrity of objects in the DTU dataset. It showcases a clear 2D output while preserving detailed geometric features, highlighting our approach's adaptability to intricate and diverse scene compositions.



Figure 10. Reconstruction Performance of UNeR3D on Real-World Anime Character Dataset: This visualization includes images from both the Coarse and Fine stages of our model, along with their corresponding depth maps. The reconstruction showcases exceptional detail in the character model, with smooth and continuous depth variations. The colors are vivid and realistic, highlighting the effectiveness of our model in handling complex real-world data with intricate details and varied textures.

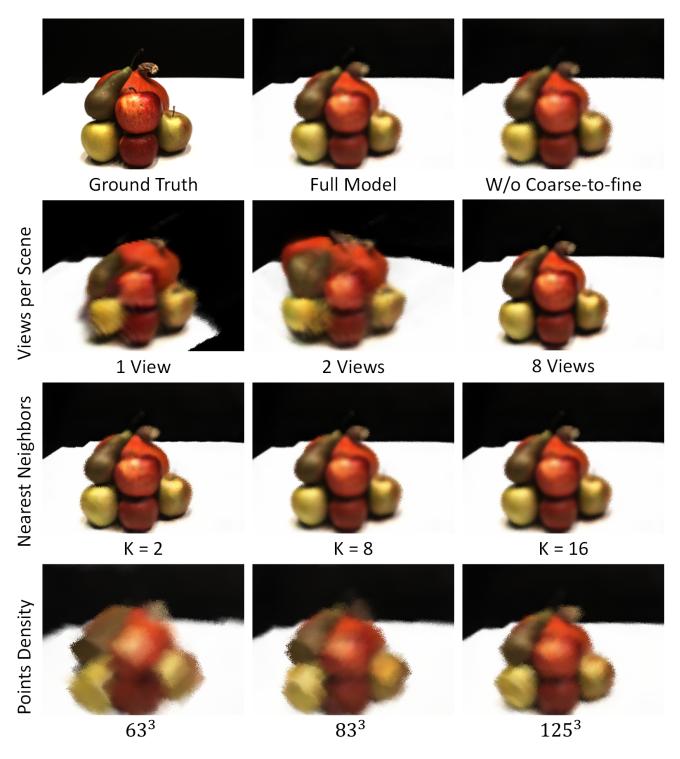


Figure 11. Comparative visualization of the ablation study results. The full model employs a coarse-to-fine structure, processes 4 input views, uses k=4 for knn, and has a resolution of 250^3 . The results demonstrate that variations in each component of our model configuration impact performance, affirming the efficacy of our approach.